Elsevier Editorial System(tm) for Journal of Structural Geology
Manuscript Draft

Manuscript Number:

Title: Use of fracture filling mineral assemblages for characterizing the formation process of an accretionary complex: an example from the Shimanto Belt southern Kyushu, Japan

Article Type: Full Length Article

Keywords: Fracture fillings, assemblage, accretionary complex, formation process

Corresponding Author: Prof. Hidekazu Yoshida, Dr

Corresponding Author's Institution: Nagoya University

First Author: Takuya Ono, Ms

Order of Authors: Takuya Ono, Ms; Hidekazu Yoshida, Dr; Metcalfe Richard, Dr

Abstract: Various kinds of fracture filling minerals and secondary minerals in the wall rocks of fractures were formed by fluid-rock interaction during the development of mélange in an accretionary complex. Each mineral formed under favourable geological conditions and can be used to estimate the conditions of accretion and formation of the mélange. Petrographic observations, mineralogical and geochemical analyses were made on fracture fillings and secondary minerals from boreholes of ca. 140 metres depth, in the Paleogene Shimanto Belt of Kyushu, Japan. Results revealed that the secondary minerals were formed in five-stages distinguished by the sequential textural relationships of the minerals and the interpreted environment of mineral formation. Filling mineral assemblages show that the studies rock formation has been subducted to a depth of several km and the temperature reached was ca. 200 - 300°C. After the subduction, the rock formation uplifted and surface acidic water penetrated up to 80 metres beneath the present ground surface. The acid water dissolved calcite fracture fillings to form the present groundwater flow-paths which allowed recent wall rock alteration to occur. The results shown here imply that filling mineral assemblages can be an effective tool to evaluate the environmental changes during and after accretionary complex formation.

20151210

Journal of Structural Geology

Dear Editor,

Here we submit a paper, entitled '**Use of fracture filling mineral assemblages for characterizing the formation process of an accretionary complex: an example from the Shimanto Belt southern Kyushu, Japan**' by Ono, Yoshida and Metcalfe with eleven figures and two tables.

This paper is the first one trying to show the usefulness of fracture fillings from deep core materials developed in the accretionary complex in order to understand the geological conditions of complex formation widely distributed in Japan as well as the feature of presently still acting as flow-paths influencing on the hydrological and engineering point of view.

I would be very grateful if you could please give this submission your consideration for publication in Structural geology.

Yours sincerely,

H. Yoshida
dora@num.nagoya-u.ac.jp
Nagoya University Museum/Graduate School of Environmental Studies
Nagoya, Aichi, Japan

Highlights

- A method using fracture fillings for understanding geological condition is proposed.
- Fracture filling assemblages are effective index for estimating the conditions.
- This method can be used for the evaluation of deep geological environment.

Journal of Structural Geology (Ono et al.)

Use of fracture filling mineral assemblages for characterizing the formation process of an accretionary complex: an example from the Shimanto Belt southern Kyushu, Japan

Takuya Ono[1], Hidekazu Yoshida[2*] & Richard Metcalfe[3]

1)Japan Atomic Energy Agency, Ibaraki, Tokai, Japan
2) Material Research Section, Nagoya University, University Museum, Chikusa, Nagoya, Japan
*corresponding author
3) Quintessa Limited, The Hub, Henley-on-Thames, Oxfordshire, UK

Abstract

Various kinds of fracture filling minerals and secondary minerals in the wall rocks of fractures were formed by fluid-rock interaction during the development of mélange in an accretionary complex. Each mineral formed under favourable geological conditions and can be used to estimate the conditions of accretion and formation of the mélange. Petrographic observations, mineralogical and geochemical analyses were made on fracture fillings and secondary minerals from boreholes of ca. 140 metres depth, in the Paleogene Shimanto Belt of Kyushu, Japan. Results revealed that the secondary minerals were formed in five-stages distinguished by the sequential textural relationships of the minerals and the interpreted environment of mineral formation. Filling mineral assemblages show that the studies rock formation has been subducted to a depth of several km and the temperature reached was ca. 200 - 300°C. After the subduction, the rock formation uplifted and surface acidic water penetrated up to 80 metres beneath the present ground surface. The acid water dissolved calcite fracture fillings to form the present groundwater flow-paths which allowed recent wall rock alteration to occur. The results shown here imply that filling mineral assemblages can be an effective tool to evaluate the environmental changes during and after accretionary complex formation.

1. Introduction

Accretionary complexes containing rock formations known as mélange are widely distributed in Japan. Understanding the process of complex formation is crucial to reveal the tectonic setting and geological evolution of the Japanese archipelago because more than 60% of the area of geology in Japan can describe as accretionary complex. The facies of mélange also has a quite complex structure with various kind of sedimentary rocks mixed in the different sedimentary conditions. In order to therefore understand the accretion conditions during terrane development distributed within Japan, various methodology estimationg the P-T conditions of complex development have been applied. As an example, a previously used methodology involved studying altered minerals in the rock matrices and fault zones that formed under relatively high P-T conditions (e.g. Tsujimori, 2010; Yamaguchi et al., 2011; Charvet, 2013). Another approach has been to determine the temperature of circulating fluid using fluid inclusions in secondary quartz veins in the rock matrices (e.g. Sakaguchi, 1999; Hashimoto et al., 2002). These methodologies, however, are limited to interpreting the evolution of relatively high P-T conditions during the development of an accretionary complex.

On the other hand, there are various kinds of fracture filling minerals and secondary minerals developed along fractures in the mélange facies. It is known that these minerals are formed from pore water squeezed from sediments during accretionary complex formation (e.g. Moore and Vrolijk, 1992). These fluids migrated under high pressure along grain boundaries and/or fractures developed in the rock. The various kinds of secondary minerals and the fracture-filling mineral assemblages record the conditions of mineral formation, and potentially can be used to trace the detailed P-T path during accretionary complex formation.

Fracture filling minerals sampled from deep bore holes drilled in crystalline rocks in Japan have been used to determine the past conditions of fluid migration and mineral formation in the Japanese orogenic field (e.g. Yoshida et al,. 2005; Yoshida et al., 2008; Nishimoto et al., 2008; Nishimoto and Yoshida, 2011; Ishibashi et al., 2014). The methodology involved identifying the minerals present in the various fracture-filling and wall-rock mineral assemblages and studying morphological relationships between the minerals. These studies have shown how the sequential order of mineral fillings and morphological relationships trace different stages of fluid circulation in crystalline host rocks and reveal the sealing process of flow-paths (Yoshida, 2012; Yoshida et al., 2013).

The study presented here aims firstly to demonstrate a methodology for evaluating the history of fluid flow through fractures in accretionary sedimentary rocks by using secondary- and fracture-filling minerals. The methodology is demonstrated by examining one of the major mélanges in an accretionary complex of the Shimanto belt of western Japan. This is the first time that this methodology has been used to determine the detailed conditions of fluid circulation during accretion and to evaluate how long the flow-paths remained open before their eventual sealing by precipitated minerals.

The methodology and the kinds of information obtained are expected to be transferable to site characterization for a variety of underground facilities. For example, should a deep un-weathered geological environment within the orogenic field of Japan be selected to site a repository for the disposal of nuclear waste, the methodology could be applied to evaluate the long-term stability of the host rock (NUMO. 2011; Committee for Geological Stability Research, 2011).

2. Studied materials and methodology

The study was carried out on the Hyuga Group, a member of the Shimanto accretionary complex, which is distributed in the southern part of the island of Kyushu. The Hyuga Group is mainly composed of bedded sandstone and sandstone-rich alternating beds of sandstone and mudstone (Figures 1a, b). Such alternating sediments are a typical feature of the Shimanto belt throughout the south-eastern part of Japan. The age of the sediments has been estimated from radiolarian fossils to range from the middle Eocene to early Oligocene (Kimura et al., 1991; JGS, 2010;). The formation is composed mainly of calcareous, greyish turbidity sequences generally dipping northwards at 30° with a strike of N55°E N. The original sedimentary textures are generally well preserved (Figure 2).

Within the studied area along the north-south trending Omaru river, five boreholes were drilled into the Shimanto sequences along an east-west line. The purpose of the boreholes was to characterize the detailed geological structure of the basement and weathering conditions, in order to determine the suitability of a proposed dam construction site. The study reported in this paper used core specimens from the five boreholes (named Core A to E; Figure 3) in order to characterize the spatial distribution of geological features with increasing depth below the ground surface, namely fracture distribution, alteration characteristics and the mineralogy of fracture fillings.

The deepest borehole 'A' reaches to 140 metres depth from the surface. Although some small fraction of the cores was lost after excavation, almost all core samples are well preserved (total recovery is about 97 %) and enable us to clarify the distribution of fractures and the occurrence of filling minerals without alteration or physical damage after exposure (Figure 4). In particular, penetration of a redox front from the ground surface can be clearly identified by the distribution of Fe-oxyhydroxide, the limits of which are marked by colour changes from reddish (oxidized rock) to grayish (reduced rock) (e.g. Akagawa et al., 2006; Yamamoto et al., 2013). The zone distinguished with Fe-oxyhydroxide occurs throughout almost the entire core or along fractures described in this paper as occurring in the shallower part of the rock sequence. This shallower part is distributed roughly parallel to the surface topography, but below the present groundwater table (Figure 3b). This is clear evidence of oxidized and/or acidic surface water infiltrating and reacting with the initially reduced greyish rocks which form the deeper part of the formation. These deeper rocks have primary fresh minerals without evidence of alteration by water infiltrating from the present ground surface (Yoshida and Yamamoto, 2014). The low temperature geochemical processes that influenced the host rock alteration can also be identified by using the morphological relationships and the mineralogical assemblages of fracture filling minerals as described below.

2.1 Fracture description

Initially the presence or absence of minerals on fracture surfaces was used to distinguish between fractures developed naturally and those developed artificially during drilling or after excavation. During the analysis, more than 3000 fractures (total 3168) were examined (Table 1). Fractures that developed naturally are characterized by fillings of euhedral crystals. On the other hand, open fractures without any fracture fillings and with the fracture surfaces exposing of fresh and clear quartz and feldspar crystal surface are readily distinguishable and formed synthetically during or after drilling or after exposure by drying and/or wetting. Such synthetically formed fractures (total 80) were excluded from the analysis of structural features that act presently as flow-paths in the mélange host rock.

Naturally formed fractures (3088) with fillings were then classified according to whether: 1) the fracture is totally sealed by filling minerals; or 2) the fracture is only partially filled by euhedral crystals and has interconnected macroscopic (visible with the naked eye) open pore space. Fractures of the first type cannot presently be acting as pathways for significant fluid movement. In contrast, fractures of the second type might act as pathways for present fluid migration. Based on the macroscopic observation of fracture fillings, the presence of euhedral crystals shows that fluids have circulated after the fracture was formed and that crystals grew on the surfaces of the wall rock without being damaged subsequently by crushing or shearing movements. Although any given borehole shows only the conditions at a particular a point on a given fracture plane, based on the large number of fracture observations it is possible to understand at least the general characteristics of the flow-path geometry developed in the mélange formation.

Fractures within the oxidized zone that developed from the ground surface (i.e. the shallower part of the studied rock sequence) and their mineral fillings have also been characterized. The fractures within this zone have Fe-oxyhydroxides within and around them. These fractures are used to determine the extent of oxidizing meteoric water penetration, as in studies of crystalline rocks at several other sites in Japan (e.g. Yoshida et al., 2013; Yamamoto et al., 2013; Yoshida and Yamamoto, 2014). Fractures formed artificially within the oxidized zone do not contain any Fe-oxhydroxides or other filling or lining minerals, and therefore are readily distinguished from the natural fractures distributed in the zone.

2.2 Morphological observations, mineralogy and geochemical characteristics

In order to analyze the morphological and structural inter-relationships among the mineral infills in the fractures, thin-sections of wall rocks and infilling minerals were prepared and optical microscopic observations were carried out. Rock thin-sections were made vertically across the fracture plane and filling minerals to clarify the textural relationships among them.

Core specimens with fillings were impregnated by epoxy resin to prevent destruction of the micro pores distributed in and around the fillings by cutting. This impregnation was necessary because the fracture fillings are quite fragile and softer than the wall rock. The impregnated specimens were thereafter carefully sliced and polished to use for optical microscopy and also for observations by scanning electron microscopy (SEM). Wavelength-dispersive x-ray (WDX) analyses were also carried out to produce chemical maps of the thin sections and thereby support the optical microscopic observations. For these SEM-WDX analyses, the thin sections observed under an optical microscope were coated with carbon by means of an ion-spattering apparatus. The WDX analyses of the coated thin sections were performed at Nagoya University Museum by using a S-3400N (Hitachi High Technologies Co. Ltd.) instrument, operated with an accelerating voltage of 15 kV.

The mineralogy of the filling minerals was determined by using X-ray diffraction (XRD). Firstly, targeted minerals were shaved from fractures using a micro-drill under an optical microscope. The shaved minerals were powdered with a mortar and a pestle. The powdered samples were then painted onto a slide glass and analyzed. The analyses were performed by a RAD-2C (Rigaku Co. Ltd.) instrument at Nagoya University Museum, with operating conditions as follows: Cu tube, Ni filter, 40 kV tube voltage, 20 mA tube current, and a scanning rate of 1 °/min.

The geochemical compositions of the mineral fillings were also analyzed by X-ray fluorescence (XRF), including ignition loss measurement, to determine the relationship between the spatial distribution of the oxidized zone and chemical composition changes in the host rock. The analyses were conducted on host rock samples a few-centimetres across and also on samples of mineral fillings exracted from the naturally opened fractures. Each sample was crushed by stamp mill and put through a sieve of 115 mesh, to produce a powder for analysis. Then, 0.5 g of powdered sample was mixed with 5.0 g lithium tetraborate and fused to produce glass beads for XRF analyses. The XRF analyses were performed by an SXF-120 instrument (Shimadzu Co. Ltd. at Graduate school of environmental studies of Nagoya University) with Rh tube, 40 kV tube voltage, and 70 mA tube current. Reference rock samples produced by the National Institute of Advanced Industrial Science and Technology (AIST) (Yamamoto and Morishita, 1999) were also used to calibrate the instrument. For the ignition loss test, the powdered samples were heated by muffle furnace at 950 °C for 3 hours.

3. Results

3.1. Fracture and oxidized zone distribution

Observations on the rock cores show that fracture frequencies vary little within the alternating sandstones and mudstones of the formation. As shown in Table 1, the average of fractures frequency identified by core observation including all sealed and open one is about 7/m through all cores from A to E (Figures 3 and 4). This finding suggests that the mechanical deformation occurred after lithification when the rocks had developed similar mechanical properties..

Open fractures are mainly identified in the shallower part, while sealed ones are distributed mainly in the deeper part (Figure 3). Open fractures of the shallower part are closely associated with Fe-oxyhydroxides that occur within the oxidized zone that occurs immediately beneath the ground surface. The maximum depth of this oxidized zone, as recognized by the deepest occurrence of Fe-oxhydroxides, reaches up to 78 metres (Core-A), 72 metres (Core-B) and 76 metres (Core-E). The core observations show that the base of the oxidized zone is almost concordant with the sedimentary layers probably due to groundwater flow along the topography and occurs deeper than present groundwater table (Figure 3b).

The chemical compositions of core-E sandstone specimens from the shallower part, as measured by XRF, show that slight movement of redox sensitive elements (e.g. Fe and Mn) and pH sensitive elements (e.g. Ca) has occurred (Table 2, Figure 5). In particular, Ca has been leached intensively at depths up to about 40 metres below the surface. This finding strongly suggests that surface water has reached at least this depth by flowing through the fracture network (Figure 5a). Due to this surface water penetration, carbonate rich fracture or pore filling minerals have been dissolved and the resulting pore spaces have remained open in the upper part of the studied rock sequence (Figure 5b). As the water was relatively oxidizing, Fe-oxyhydroxides were precipitated in and around the pore spaces. The relatively acidic water also resulted in the formation of smectite. Microscopic observations of mineral textures confirm that the Fe-oxyhydroxides and smectite were formed during the last stage of fracture evolution (Figures 5c, d).

A comparison of fracture fillings between the deeper un-oxidized zone and shallower oxidized zone in the same fracture clearly show that dissolution of the calcite filling accompanied oxidation of the rock (Figures 5e, f). The detailed process of oxidized zone formation and the reaction with the fillings are discussed following section.

3.2. Fracture fillings of deeper part

Fractures distributed deeper than the oxidized zone are almost sealed and less than 10% of the fractures without Fe-oxyhydroxides remain open. In other words, almost 90% of fractures observed in the cores are sealed without any evidence of functioning of groundwater flow. The minerals and mineral textures identified in each fracture in the deeper, unoxidized part of the studied rock sequence are shown in Figure 6. Fractures (Figures 6a - c) have various sealing minerals, primarily ankerite, siderite and quartz. Fractures having open pore space lined by quartz and ankerite are also identified and are possibly able to conduct water (Figures 6 d - f).

First of all, siderite is only identified as a mineral fill in pore spaces formed during ductile deformation (Figure 6a). Ankerite is sometimes associated with the siderite in ductile deformation structures (Figure 6b). It is presumed that the fractures formed when much of the rock matrix was still able to deform plastically. Other minerals are seen only within the pore spaces of fractures formed by brittle deformation, after the lithification of the sediments due to high-pressure compaction during accretion. The different mineral fillings in different kinds of fracture clearly enable a distinction to be made between different stages of fracturing and mineral formation under different conditions.

The minerals observed in each fracture basically grew from both walls of the fracture until they met at the centre of the fracture, thereby occluding almost all the open space. Although almost 90 % of the fractures are sealed by calcite, the remaining 10% or so of the voids volume in the fractures remained open and was able to conduct fluids.

Fine network texture veins of siderite and ankerite , without euhedral crystals, formed penetrating the muddy fine layers. The morphology of veins with uneven boundaries between the vein and the host rock matrices show that the fillings formed before the matrix was fully consolidated (Figures 7a, b). On the other hand, within the open space of fractures that formed within consolidated rock quartz crystals (Figures 8a, b) grew on the wall rock directly. In these cases, sometimes euhedral ankerite (Figures 8c, d) and fibrous siderite cover the quartz crystals. Calcite crystals formed on these fillings (Figures 8e, f) showing and is not overgrown by any later minerals; this calcite represents the latest stage of mineralisation (Figures 7c, d). The euhedral form of the calcite is a quite specific feature readily identified by SEM observations, suggesting the pore space and/or opened fractures are still acting as flow-paths for ground water movement, as is also known in the case of deep crystalline rocks distributed in Japan (e.g. Yoshida et al., 2013).

Illite is seen in the wall rocks along fractures filled by un-deformed quartz (Figure 7e) and feldspar grains (Figure 7f). This implies that the illite was formed during the circulation of hydrothermal fluids and simultaneously the fluids precipitated the quartz crystals on the pore surfaces of the fracture.

4. Discussion

4.1. Formation stage of filling and alteration minerals

The morphological and textural relationships of fracture fillings and secondary minerals in the rock matrices, suggest that the following stages of mineralisation occurred during the development of the accretionary complex and the subsequent uplift of the rock.

Stage I

Stage I is characterized by siderite and ankerite fillings in pore space that formed during the ductile deformation of unconsolidated sediment (Figures 7a, b). Pores filled with these minerals without forming crystal texture with a restricted distribution in mudstone layers and do not cut across the sedimentary structure. These pores show pinch-and-swell structures, and composite planar fabrics with the Y surfaces parallel to sedimentary structures (Figures 6a, b). Also almost no alteration occurs along the margins of the matrix pores that are filled with ankerite and siderite. This observation suggests that the pore fillings are authigenic and formed concordantly with the ductile pore geometry, probably soon after the sediments subducted, but before their consolidation.

The fluid involved in the formation of siderite and ankerite in Stage I is interpreted to have been enriched in Ca and Mg, and probably was expelled from the muddy layers due to squeezing during accretion, as suggested by the structures shown in Figures 6a, b. Moreover, the fracture with a pinch-and-swell structure and Y-P fabrics suggests that the fracturing progressed by layer-parallel shearing (e.g. Kano and Murata, 1998; Ben et al., 2002). Such ductile deformation resulting in the pinch-and-swell structures also show that the rock body was still unconsolidated and had relatively high porosity during the early stage of the accretion process. This interpretation is also supported by the quartz grains in the rock matrices showing no deformation (Figures 7e).

It is known that siderite is generally formed during diagenesis under reducing conditions at temperatures less than about 100 ^{o}C (e.g. Mohamed et al., 2006). Kondo et al. (2005) has also been reported that, based on fluid inclusion measurements, sheared ankerite in fractures around shear zones or thrust zones in the Shimanto Belt within the same area of Kyushu is estimated to have formed at a temperature of 100 – 250 °C.

Stage II

Stage II is characterized by quartz fillings within the porosity of fractures developed under conditions of relatively high pressure and high temperature (Ohira et al., 2010). This quartz typically forms euhedral columnar crystals that cover the fracture surfaces (Figures 8a, b). Fractures with this type of quartz commonly have planar fracture surfaces and cut sedimentary layers at high angles (Figures 6c, d). Within the rock matrices along the same fractures, illite was formed in and around feldspar grain boundaries (Figure 7f), probably due to the circulation of relatively high temperature hydrothermal fluids.

The planar shape fractures with quartz fillings developed in Stage-II cross-cut the sedimentary layers that were deformed in Stage-I (Figures 6c, d), thereby showing that the Stage II fractures formed after the had sediments completely solidified. In particular, euhedral crystals on the planar fracture surfaces indicate that fracturing developed open pore space sufficient for mineral growth (e.g. Nicholas and Paul, 2001). These features suggest that the fractures formed after the stress had started to decrease, probably due to unloading during uplift of the consolidated sediments.

Based on measurements of homogenisation temperatures on fluid inclusions within the euhedral quartz it has been estimated that the geothermal fluids from which the quartz precipitated had temperatures in the range 80 – 300 °C (e.g. Muramatsu, 1987; Ohira et al., 2010). XRD analyses on illite in samples from the altered zone around the fractures with quartz fillings (Figures 9a, b) and the mode of occurrence of the illitized plagioclase, are quite similar to illitized plagioclase formed along flow-paths within crystalline rock by geothermal activity (Nishimoto and Yoshida, 2010). The illite in such situations is most likely to have formed within the temperature range 200 – 300 °C (e.g. White and Hedenquist, 1995). Stage-II is therefore interpreted to have formed later than Stage I, at relatively high pressure and temperature, during uplift that accompanied the accretion process after maximum depths had been attained.

Stage III

Stage III is characterized by ankerite crystals with euhedral rhombic shapes, which are in contrast to the microcrystalline ankerite crystals identified in Stage-I. Since the euhedral ankerite crystals cover the Stage-II columnar quartz (Figures 8c, d), the stage clearly post-dates Stage I and II. Fractures formed in Stage-III have form a network and/or branching structure and cut the fractures formed in Stage-II (Figures 6e, f). However, there is almost no alteration identified along the fractures, suggesting that the geothermal fluids from which the Stage III ankerite precipitated had lower temperatures than those of the geothermal fluids that formed the Stage II mineralisation.

The mode of occurrence of the branching fractures, the fillings of which contain fine fragments of wall rock, suggest that the pore fluid pressure was still relatively high during fracturing and mineral filling formation, probably close to lithostatic pressure, (e.g. Yoshida et al., 2013). Fractures with euhedral Mg-rich carbonates have been reported from hydrothermally altered limestone and their formation temperature has been estimated to have been between 100 – 280 °C (Tritlla et al., 2001; Chen et al., 2004; Luczaj et al., 2006). Saller (1984) has also reported Mg-rich carbonate precipitations from modern Pacific Ocean water at deeper than 1,000 metres depth with relatively high temperature condition.

As the sediments had already consolidated by the time that Stage III mineralisation formed, the source of the Mg that became incorporated into this mineralisation was unlikely to have been water squeezed from the rock matrix. It is more likely that the Mg was supplied by another process. One possibility is that, during stage III, during continuing uplifting, seawater might have penetrated through the open fractures and provided the Mg that became incorporated into the Stage III fracture-filling minerals.

Stage IV

This stage is characterized calcite that seals up to ca. 90% of the pore-space that remained in the fractures following the fracturing and mineralisation of Stages I ~ III. The calcite in this stage typically shows euhedral shapes (Figures 8e, f) and covers or develops on the quartz and ankerite fillings formed in Stage-II and Stage-III respectively (Figures 7c, d). Such a textural relationship is also shown by WDX analysis (Figure 10) and suggests that the calcite of Stage IV post-dates the other stages and healed the remaining fracture porosity.

Fracture-filling and diagenetic calcite from various locations was estimated to have formed over a wide range of temperature, between 60 – 240 ^{o}C (e.g. Muramatsu, 1987; Sakaguchi, 1999; Blyth et al., 2000). However, there is no major alteration developed in the wall-rocks of fractures adjacent to Stage IV mineralisation, implying that this mineralisation formed towards the lower end of this temperature range. Without groundwater chemistry data, it is rather difficult to estimate the origin of the Ca and the fluids from which the Stage IV calcite circulated. However, calcite is a common fracture-filling mineral along pathways for present groundwater flow identified at depths of up to 1,000 metres in granitic rocks studied in underground facilities excavated in central Japan (e.g. Yoshida et al., 2013; Ishibashi et al., 2014). Indeed these previous studies have revealed that the calcite mineralisation can be used as an indicator of flow-paths presently conducting groundwater circulation.

The detailed observations identified various shapes of calcite crystals in the Stage IV mineralisation. It is possible that these morphological changes reflect changes in pore water salinity caused by mixing between old seawater and more recent, fresh meteoric water; more elongate crystals tend to precipitate from more saline water (e.g. Iwatsuki et al. 2002). Possibly the source of the Ca in the calcite of stage IV was seawater that infiltrated the formation during uplift.

Stage V

Stage V is characterized by Fe-oxyhydroxides that coat fracture surfaces. Fractures showing this stage of mineralisation are developed dominantly within the shallower part of the studied sequence (i.e. the oxidized zone). In particular, Fe-oxyhydroxides occur in fractures from which calcite fillings have been dissolved, probably due to the penetration of relatively acidic, fresh meteoric water (Yamamoto et al., 2013; Figures 5e, f). Microscopic observations on rock samples from the oxidized zone also show that plagioclase has altered to smectite, again consistent with the penetration of meteoric water (Figure 5d).

Stage V is therefore interpreted as the final stage of fracture mineralisation, that formed after the sedimentary formation had approached the ground surface, or after exposure at the ground surface. The Fe-oxyhydroxides could have been formed as a consequence of the pH increase that would have occurred as the acidic meteoric water dissolved calcite and reacted with feldspar to form smectite. This redox reaction developed the oxidized zone recognized from the distribution of Fe-oxyhydroxides along fractures at depths of up to several tens of metres beneath the ground surface, as shown in a cross section through this site (see Figure 3). The temperature of smectite formation in other sedimentary sequences has been estimated to have been lower than 100 °C (e.g. White and Hedenquist, 1995). Formation of fracture-lining Fe-oxyhydroxides and related smectite alteration of granitic rock under near-surface conditions was also investigated along water conducting fractures in a fault zone in granitic rock (e.g. Nagatomo and Yoshida, 2009).

The mineralisation stages developed during accretion of the Hyuga Group and their estimated conditions of formation are summarized in Figure 11. Based on the filling mineral assemblages and the deformation features of the fractures, it is suggested that the accretion depth of the Hyuga Group was shallower than reported for the same Shimanto complex further to the east, in the Kii area of central Japan (e.g. Hashimoto et al., 2002). Filling minerals seen in the Kii area are epidote and chlorite, which indicate that mineralisation in the Kii area occurred under higher formation temperatures and/or pressures than the fracture-filling minerals of the study area considered in this paper. These differences also support the use of mineral assemblages to distinguish how the same accretionary complex subducted under different geological conditions.

4.2. Redox front development from the ground surface

The characteristics of fracture fillings in the shallower part of the studied rock sequence (i.e. the oxidized zone) show that meteoric water has penetrated along fractures and reacted with the calcareous sandstone wall rocks to a depth of at least 80 metres beneath the present ground surface. Microscopic features of the fracture mineralisation reveal that the calcite filling formed in Stage IV has been almost totally dissolved and Fe-oxyhydroxides have formed on the surfaces exposed by the loss of calcite. The calcite dissolution developed flow-paths which facilitated circulation of meteoric water, penetrating from the ground surface. This is the first time for a melange sequence that original fluid flow paths have been distinguished from secondary ones formed as a result of meteoric water penetration. Such a distinction should be taken into account for understanding the suitable depth of facility allocation when undertaking hydrological and geotechnical investigations for siting of any relevant underground facility used e.g. for radioactive waste disposal in Japan.

The behaviour of Ca, Mn and Fe in the fractured rocks, as measured by the XRF analyses, imply that the infiltrating water was acidic but not of such low pH that it could not be buffered to more alkaline pH by water / rock reactions, causing fixation of Fe as Fe-oxyhydroxide. The source of such acidic water could have been pore water in soils covering the basement rock. Soils in general tend to be rich in organic acid, due to decomposition of organic materials (Küsel et al., 2002; Petrunic et al., 2005).

The characteristics of the oxidized zone in the shallower part of the studied rock sequence is quite similar to oxidized zones in crystalline rocks, which are interpreted to have been controlled by the pH-buffering effect of water / rock reactions (Yamamoto et al., 2013). These studies of crystalline rocks concluded that the source of the Fe fixed in the Fe-oxyhydroxides was the overlying soils, based on the observation that Fe has been gained by the oxidized zone in the granitic rock. However, in the case of the Shimanto, XRF data for the calcareous sedimentary rocks show almost no Fe accumulation in the oxidized zone. This shows that any Fe dissolved from the soil or near-surface rock-forming minerals probably precipitated soon just after dissolution and did not migrate far. Such differences between the cases of crystalline rocks and the Shimanto sedimentary rocks are explained by the relatively high potential for pH buffering of the Hyuga Group. This relatively high buffering capacity is provided by the high abundance of carbonate cement in the fractures and sedimentary matrices. Such differences in buffering capacity are important considerations when assessing the potential barrier function of the geological environment surrounding underground waste disposal facilities, for example for the disposal of nuclear wastes.

5. Conclusion

The modes of occurrence, mineralogical assemblages and geochemistry revealed that fracture filling minerals in the studied Hyuga Group mélange were formed in five-stages, each one distinguished by the sequential textural relationships of the minerals and the interpreted environment of mineral formation. Stage I: fibrous siderite and ankerite precipitated in a muddy matrix formed before sediment consolidation; Stage II: euhedral quartz precipitated from high-temperature hydrothermal fluids circulating within the open pore space of fractures and at the same time the fluids altered plagioclase in the wall rocks; Stage III: euhedral ankerite grew on minerals formed in Stage II; Stage IV: euhedral calcite growth was caused by meteoric water penetration and sealed most of the fractures up to ca. 90%; Stage V: calcite dissolved and Fe-oxyhydroxides precipitated due to infiltration of acidic meteoric water that percolated through organic rich soil. The dissolution front reaches a depth of about 70 metres below the present ground surface. Within the five stages, the mineralogical assemblages suggest that Stage-II was developed under the highest temperature conditions, ca. 200 – 300 °C, during the period when the rock mass was buried to depths of at least several km. The results shown here imply that the use of mineral assemblages formed in fractures can be an effective tool to evaluate the collision processes and the environmental changes during accretionary complex formation. The observations can also be used to develop a predictive model for the present spatial distribution features of the rock mass that may conduct flowing groundwater. Such a predictive model is important for developing various kinds of underground facilities, such as waste repositories.

Acknowledgments

We are grateful to Dr. Y. Nishizono and Mr. A. Oshima of West Japan Engineering Consultants, Inc. for their helpful sample preparation and advices over all of this study. We also thank to Prof. M. Takeuchi, Prof. K. Yamamoto, Lecturer Dr. Y. Asahara of Nagoya University for their discussion and support on geochemical analysis during the research. Ms.M. Nozaki, Mr. S. Yogo of the Nagoya University Museum and Dr. S. Nishimoto of Nagoya City Science Museum for their technical supports and advice during observations and analysis.

Captions

Figure 1 Index map of the distribution of Shimanto accretionary complex and studies site (a). Geological map around the dam site along Omaru river (b) modified after Kimura et al. (1991).

Figure 2 Sandstone hosted formation of Hyuga group occurred in the dam site. Well layered formation (a) and mudstone rick part (b).

Figure 3 Detailed surface geology with location of bore hole drillings (a). Geological cross section along the boreholes (b). Red coloured zone of shallower part identified as oxidized zone with open fractures and blue coloured deeper part characterized by the sealed fractures.

Figure 4 Occurrence of the core specimens drilled at the dam site (Core-B) from the surface to depth of 75 metres. Shallower part is identical with the reddish colour by ferric iron precipitation due to surface acidic water penetration.

Figure 5 Depth profile of major elements according the XRF data shown in Table 2 (a). The feature of $CaCO_3$ dissolution at the oxidation front (b). Photomicrograph shows the Fe-oxyhydroxides precipitation in and around the $CaCO_3$dissolved fractures (c, d) and the $CaCO_3$ filled pores and dissolved pores due to acidic surface water penetration cross the reaction front (e, f).

Figure 6 Occurrences of fracture fillings of different stages identified in the host rock. Siderite and ankerite veins in muddy layers without cutting sedimentary layers (Stage-I) (a,b). Quartz vein cut sedimentary structure showing brittle fracturing after consolidation of sediments (Stage-II) (c,d). Ankerite with euhedral crystal filling identified in the opened brittle formed fracture (Stage-III) (e, f).

Figure 7 Photomicrograph of optical microscope (cross) of veins and matrix. Siderite and ankerite fillings within the host-rock sedimentary layer without clear boundary between fillings and matrix suggesting still unconsolidated facies remained the veins were formed recognized as Stage-I (a, b). Illite precipitated within micro-pores in the matrix probably due to high temperature fluid circulation defined as Stage-II (e, f). Occurrence of carbonate ($CaCO_3$) clearly showing the latest stage filled all previously formed fillings as Stage-IV (c, d).

Figure 8 SEM micrographs of fillings identified in the opened fractures. Euhedral quartz formed identified in the opened fractures of Stage-II (a, b). Euhedral ankerite covering on euhedral quartz of Stage-II identified as the Stage-III (c, d). Various shape of calcite crystals forming on the fillings previously formed as defined as Stage-IV (e, f).

Figure 9 XRD patterns of unaltered host rock and hydrothermally altered host rock (a) and the filling of calcite and without calcite comparing cross the acidic water penetration in the same fracture (b).

Figure 10 Micrograph of SEM (a) and WDX mappings (b ~ d) of Ca, Fe and Mg cross the fillings clearly showing the compositional differences of filling and precipitated order distinguishable the each Stage.

Figure 11 Summarised configuration of accretionary complex forming constructed by using secondary fracture filling minerals assemblage and the conditions estimated in each Stage.

Table 1 Fracture frequencies (number of fractures identified: 3168) of all drilled cores (A - E) and showing the depth of shallower part identified by reddish coloured by Fe-oxyhydroxides.

Table 2 XRF data of host rock taken from deepest drilled Core-E from the surface to the depth of 115.8 metres.

References

Akagawa, F., Yoshida, H., Yogo, S., Yamamoto, K., 2006. Redox front formation in fractured crystalline rock: an analogue of matrix diffusion in an oxidizing front along water-conducting fractures. Geochemistry: Exploration, Environment, Analysis, 6, 49–56.

Ben, D. G., Cees, W. P., Martin, H., 2002. Boudinage classification: end-member boudin types and modified boudin structures. Journal of Structural Geology, 26, 739–763.

Blyth, A., Frape, S., Blomqvist, R., Nissinen, P., 2000. Assessing the past thermal and chemical history of fluids in crystalline rock by combining fluid inclusion and isotopic investigations of fracture calcite. Applied Geochemistry, 15, 1417–1437.

Charvet, J., 2013. Late Paleozoic-Mesozoic tectonic evolution of SW Japan: A review – reappraisal of the accretionary orogeny and revalidation of the collisional model. Journal of Asian Earth Science, 72, 88–101.

Chen, D., Qing, H., Yang, C., 2004. Multistage hydrothermal dolomites in the Middle Devonian (Givetian) carbonates from the Guilin area, South China. Sedimentology, 51, 1029–1051.

Committee for Geological Stability Research, 2011. Geological Leaflet 4, Japanese Island-arc and Geosphere Stability. The Geological Society of Japan, No.4.

Hashimoto, Y., Enjoji, M., Sakaguchi, A., Kimura, G., 2002. P-T conditions of cataclastic deformation associated with underplating: An examples from the Cretaceous Shimanto complex, Kii Peninsula, SW Japan. Earth Planets Space, 54, 1133–1138.

Ishibashi, M., Ando, T., Sasao, E., Yuguchi, T., Nishimoto, S., Yoshida, H., 2014. Characterization of water conducting fracture and their long-term behavior in deep crystalline rock: a case study of the Toki Granite. Journal of the Japan Society of Engineering Geology. 55, 156–165.

Iwatsuki, T., Satake, R., Metcalfe, H., Yoshida, H., Hama, K., 2002. Isotopic and morphological features of fracture calcite from granitic rocks of the Tono area, Japan: a promising paleohydrogeological tool. Applied Geochemistry, 17, 1241–1257.

JGS (The Geological Society of Japan), 2010, *Nihon chihou chishitsu shi* [Local Geology of Japan] 8, The Kyushu and Okinawa Area. Asakura Shoten, Tokyo.

Kano, K., Murata, A., 1998. *Kouzou chishitsu gaku* [Structural geology]. Asakura Shoten, Tokyo.

Kimura, K., Iwaya, T., Mimura, K., Sato, Y., Sato, T., Suzuki, Y., Sakamaki, Y., 1991. Geology of the Osuzuyama Distinct (with Geological Sheet Map at 1:50,000). Geological Survey of Japan, Tsukuba.

Kondo, H., Kimura, G., Masago, H., Ohmori-Ikehara, K., Kitamura, Y., Ikesawa, E., Sakagchi, A., Yamaguchi, A., Okamoto, S., 2005. Deformation and fluid flow of a major out-of-sequence thrust located at seismogenic depth in an accretionary complex: Nobeoka Thrust in the Shimanto Belt, Kyushu, Japan. Tectonics, 24, TC6008.

Küsel, K., Wagner, C., Trinkwalter, T., Gössner, A. S., Bäumler, R., Drake, H. L., 2002. Microbial reduction of Fe(III) and turnover of acetate in Hawaiian soils. FEMS Microbiology Ecology, 40, 73–81.

Luczaj, J. A., Harrison III, W. B., Williams, N. S., 2006. Fractured hydrothermal dolomite reservoirs in the Devonian Dundee Formation of the central Michigan Basin. AAPG Bulletin, 90, 1787–1801.

Mohamed, A. K. E., Howri, M., Sadoon, M., Ihsan, A. A., George, A., 2006. Distribution of diagenetic alterations in fluvial and paralic deposits within sequence stratigraphic framework: Evidence from the Petrohan Terrigenous Group and the Svidol Formation, Lower Triassic, NW Bulgaria. Sedimentary Geology, 190, 299–321.

Moore, J. C., Vrolijk, P., 1992. Fluids in accretionary prisms. Reviews of Geophysics, 30, 113–135.

Muramatsu, Y., 1987. Distributions, paragenesis and fluid inclusions of hydrothermal minerals in the Kakkonda geothermal field, Northeastern Japan. Journal of mineralogy, petrology and economic geology, 82, 216–229.

Nagatomo, A., Yoshida, H., 2009. Analysis of the geological history of the active Atera Fault, central Japan, based on fault and fracture systems and infilling minerals. Journal of geological society of Japan, 115, 512–527.

Nicholas, H. S. O., Paul, D. B., 2001. Mechanisms of fluid flow and fluid-rock interaction in fossil metamorphic hydrothermal systems inferred from vein-wallrock patterns, geometry and microstructure. Geofluids, 1, 137–162.

Nishimoto, S., Ukai, E., Amano, K., Yoshida, H., 2008. Analysis of alteration process of deep granitic rock – A case study of Toki granitic rock-. Journal of Engineering Geology of Japan, **49**, 94-104.

Nishimoto, S., Yoshida, H., 2010. Hydrothermal alteration of deep fractured granite: Effects of dissolution and precipitation. Lithos, 115, 153–162.

Nuclear Waste Management Organization of Japan (NUMO), 2011. Safety analysis of Nuclear waste disposal, NUMO-TR-11-01.

Ohira, H., Nagai, R., Nishizaka, R., Takeuchi K., 2010. Fluid inclusion and thermal history of the Izumiyama pottery stone deposit, Arita distinct, Saga Prefecture. Fission track news letter, 23, 4–6.

Petrunic, B. M., MacQuarrie, K. T. B., Al, T. A., 2005. Reductive dissolution of Mn oxides in river-recharged aquifers: a laboratory column study. Journal of Hydrology, 20, 163–181.

Sakaguchi, A., 1999. Thermal maturity in the Shimanto accretionary prism, southwest Japan, with the thermal change of the subducting slab: fluid inclusion and vitrinite reflectance study. Earth and Planetary Science Letters, 173, 61–74.

Saller, A. H., 1984. Petrologic and geochemical constraints on the origin of subsurface dolomite, Enewetak Atoll: An example of dolomitization by normal seawater. Geology, 12, 217–220.

Tritlla, J., Cardellach, E., Sharp, Z. D., 2001. Origin of vein hydrothermal carbonates in Triassic limestones of the Espdán Ranges (Iberian Chain, E Spain). Chemical Geology, 172, 291–305.

Tsujimori, T., 2010. Paleozoic subduction-related metamorphism in Japan: new insights and perspectives. Journal of Geography, 119, 294–312.

White, N. C., Hedenquist, J. W., 1995. Epithermal gold deposits: styles, characteristics and exploration. Published in SEG Newsletter, 23, 9–13.

Yamaguchi, A., Cox, F. Stephan, Kimura, G., Okamoto, S. 2011. Dynamic changes in fluid redox state associated with episodic fault rupture along a megasplay fault in a subduction zine. Earth and Planetary Science Letters, 302, 369-377.

Yamamoto, K., Yoshida, H., Akagawa, F., Nishimoto, S., Metcalfe, R., 2013. Redox front penetration in the fractured Toki Granite, central Japan: An analogue for redox reactions and redox buffering in fractured crystalline host rocks for repositories of long-lived radioactive waste. Applied Geochemistry, 35, 75–87.

Yoshida, H., Takeuchi, M., Metcalfe, R., 2005. Long-term stability of flow-path structure in crystalline rocks distributed in an orogenic belt, Japan. Engineering Geology, **78**, 275-284.

Yoshida, H., Nishimoto, S., Cho, A., Yamamoto, K., Katsuta, N., 2008. Alteration of subsurface granitic rock in Okayama area, Japan, Journal of Engineering Geology of Japan, **49**, 256-265.

Yoshida, H., 2012. Fluid Conducting Fractures and Their Long-term Behavior in Crystalline Rocks: Present Understanding and Future Perspectives. Journal of Geography, **121**, 68-95.

Yoshida, H., Metcalfe, R., Ishibashi, M., Minami, M., 2013. Long-term stability of fracture systems and their behavior as flow paths in uplifting granitic rocks from the Japanese orogenic field. Geofluids, 13, 45–55.

Yoshida, H., Yamamoto, K., 2014. Fe oxyhydroxides in underground geological environments and high-level radioactive waste disposal: Analysis of influence on nuclide migration scenarios. Journal of Geological Society of Japan, 120, 327−343.

Figure 1

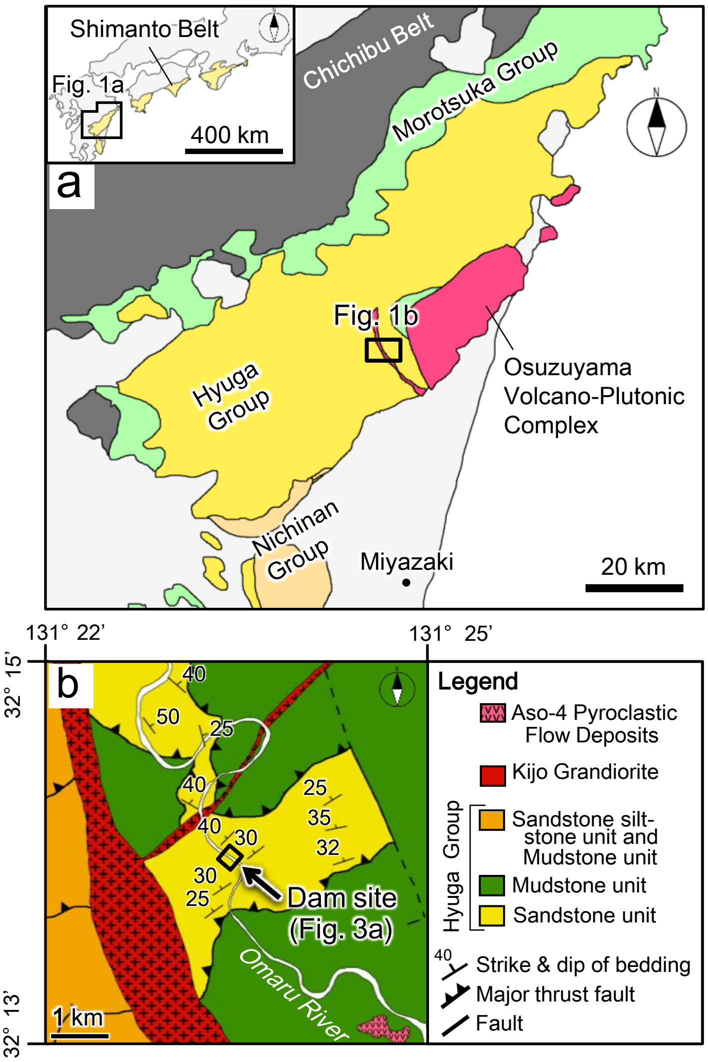

Figure 1

Figure 2

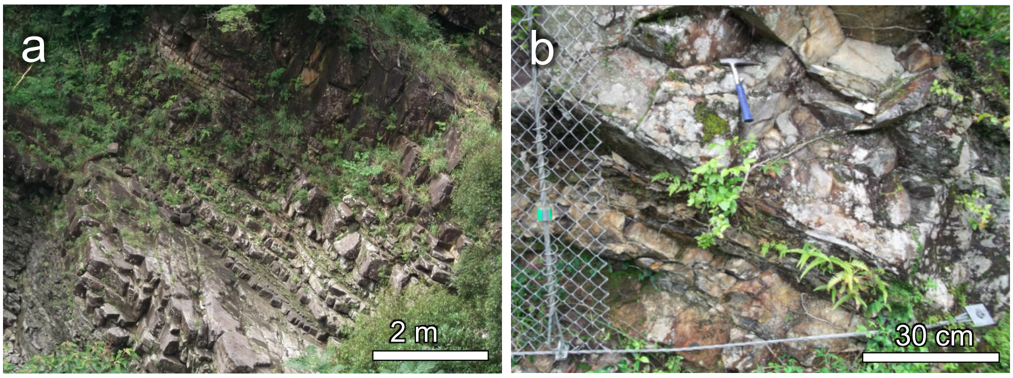

Figure 2

Figure 3

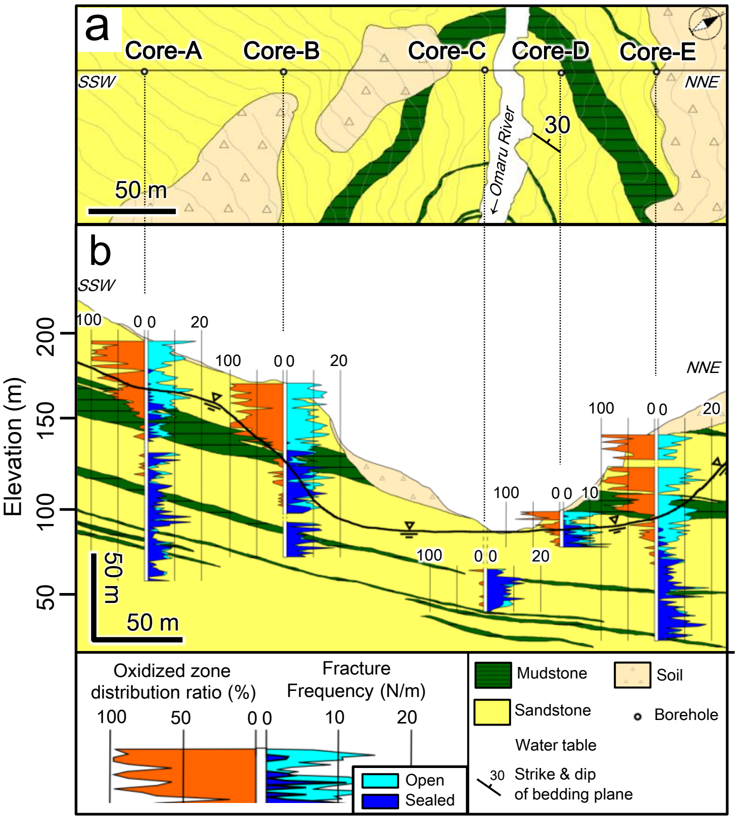

Figure 3

Figure 4

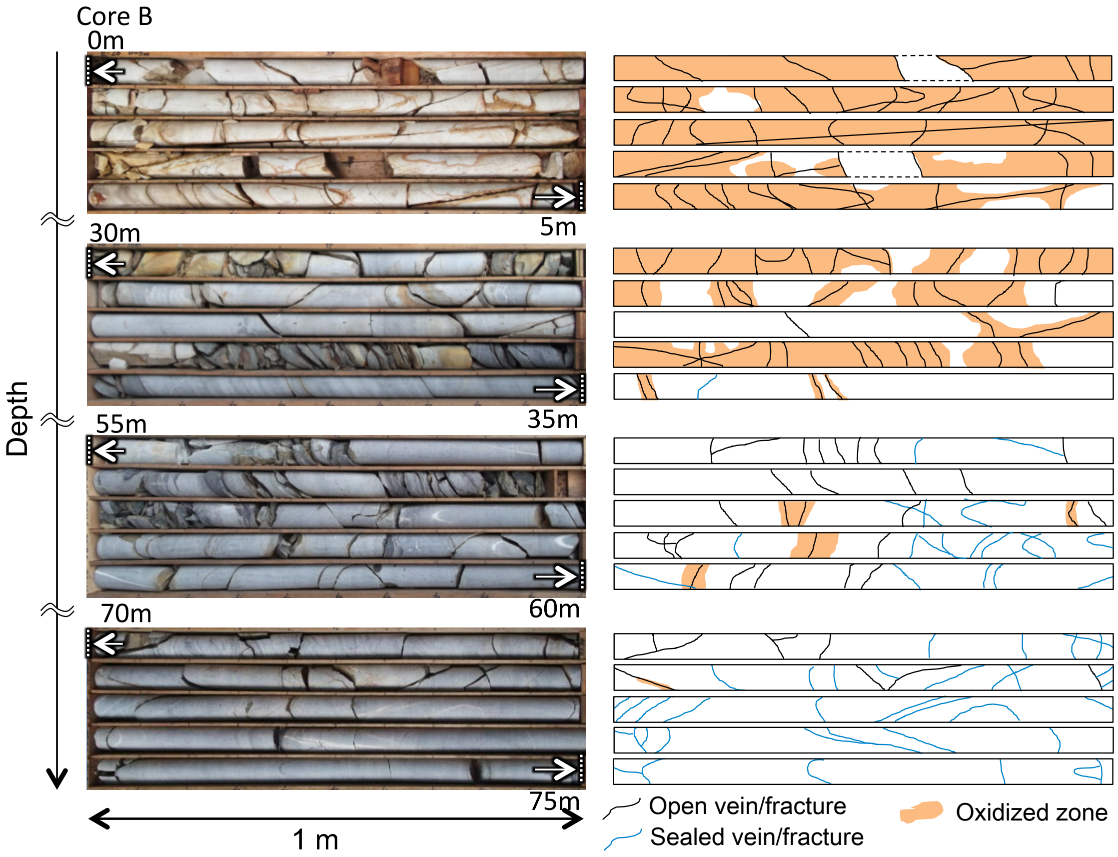

Figure 4

Figure 5

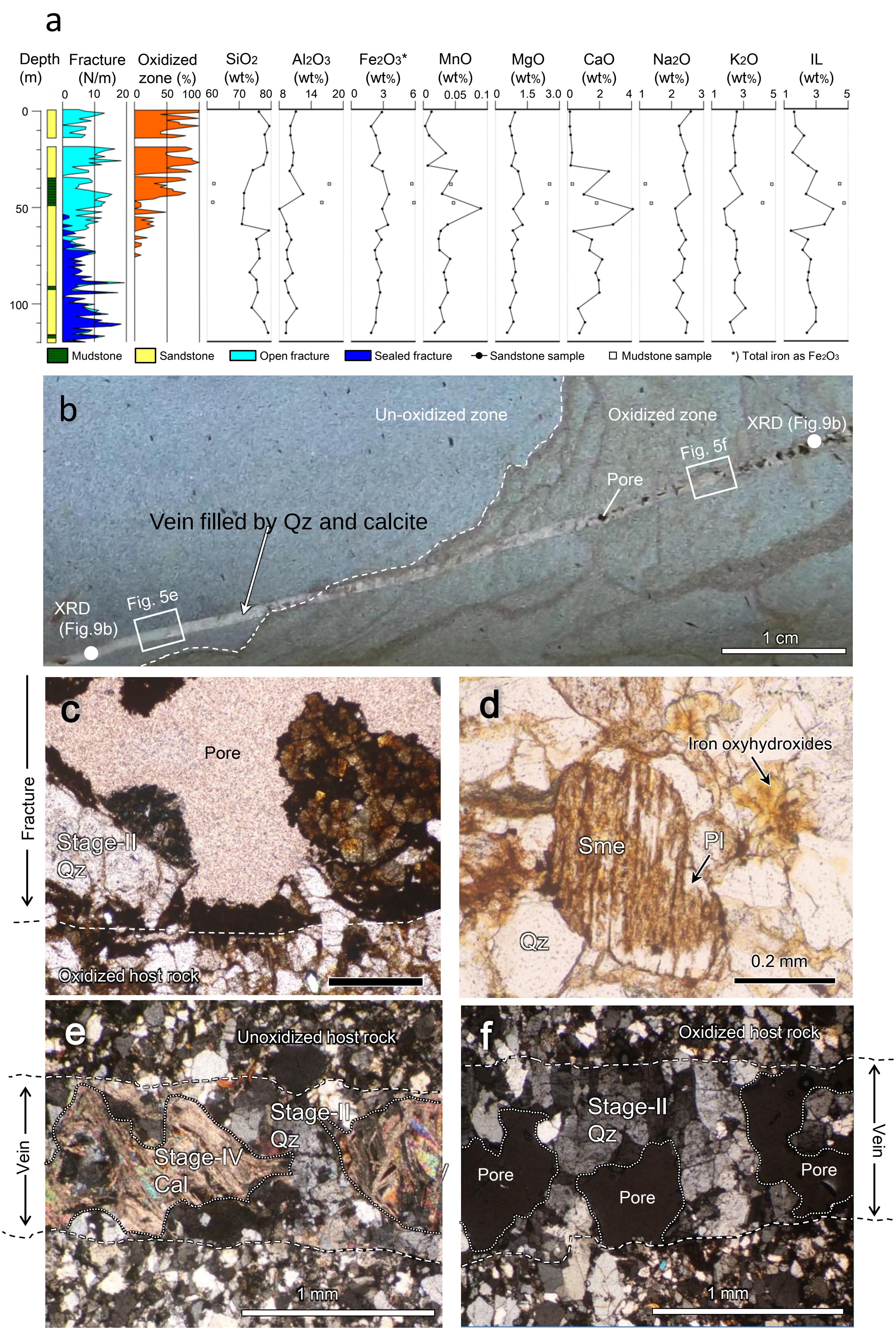

Figure 5

Figure 6

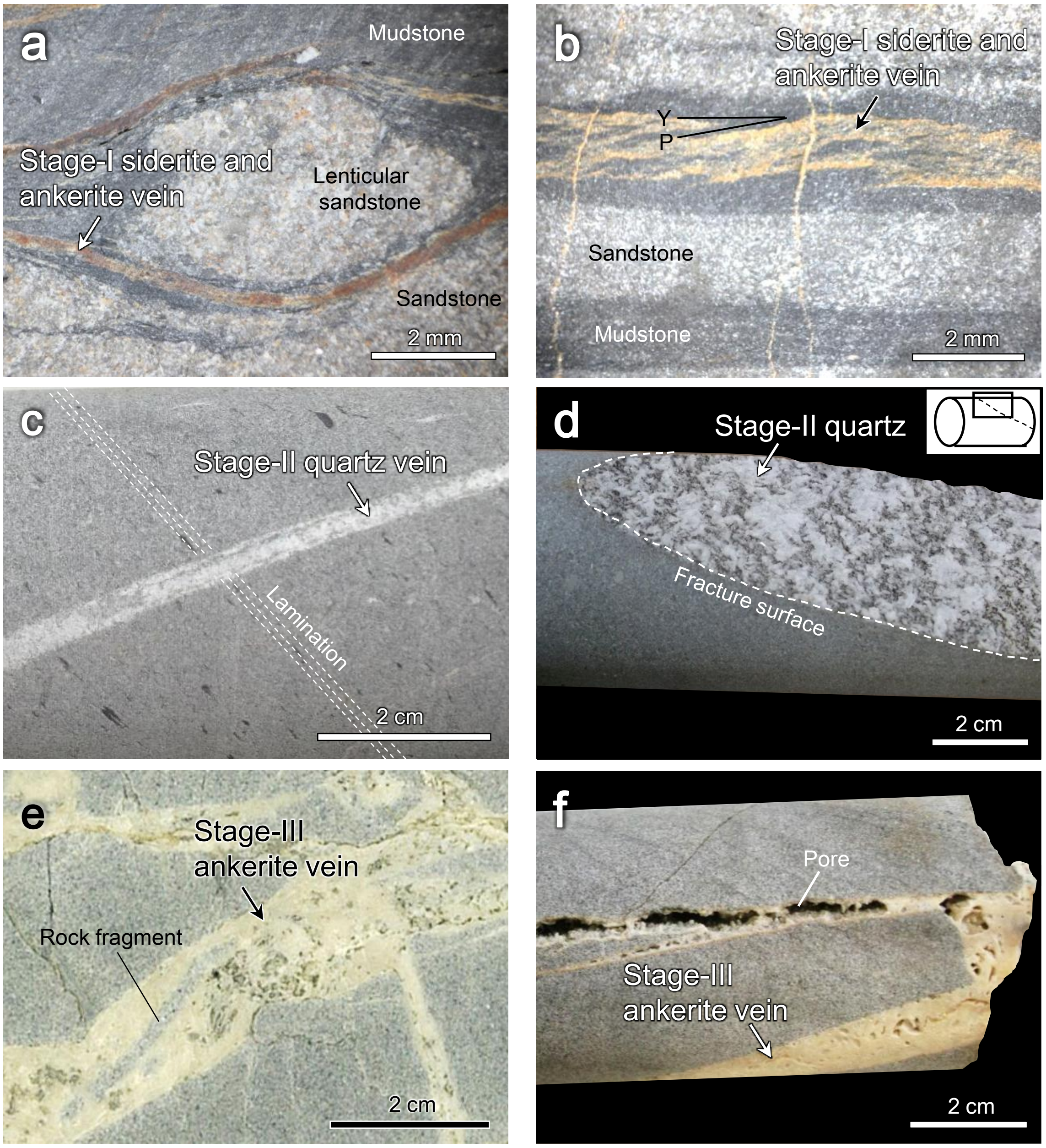

Figure 6

Figure 7

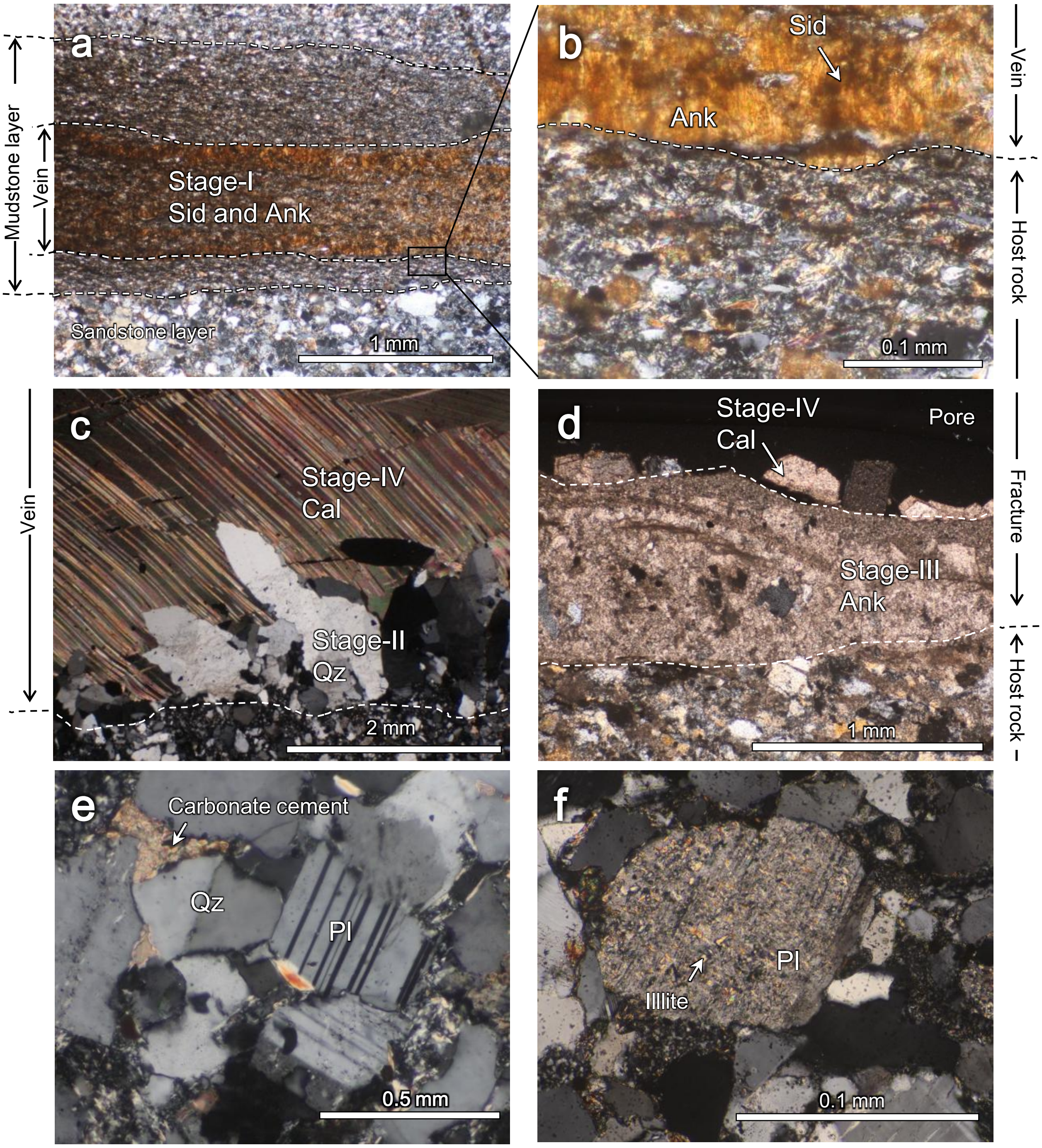

Figure 7

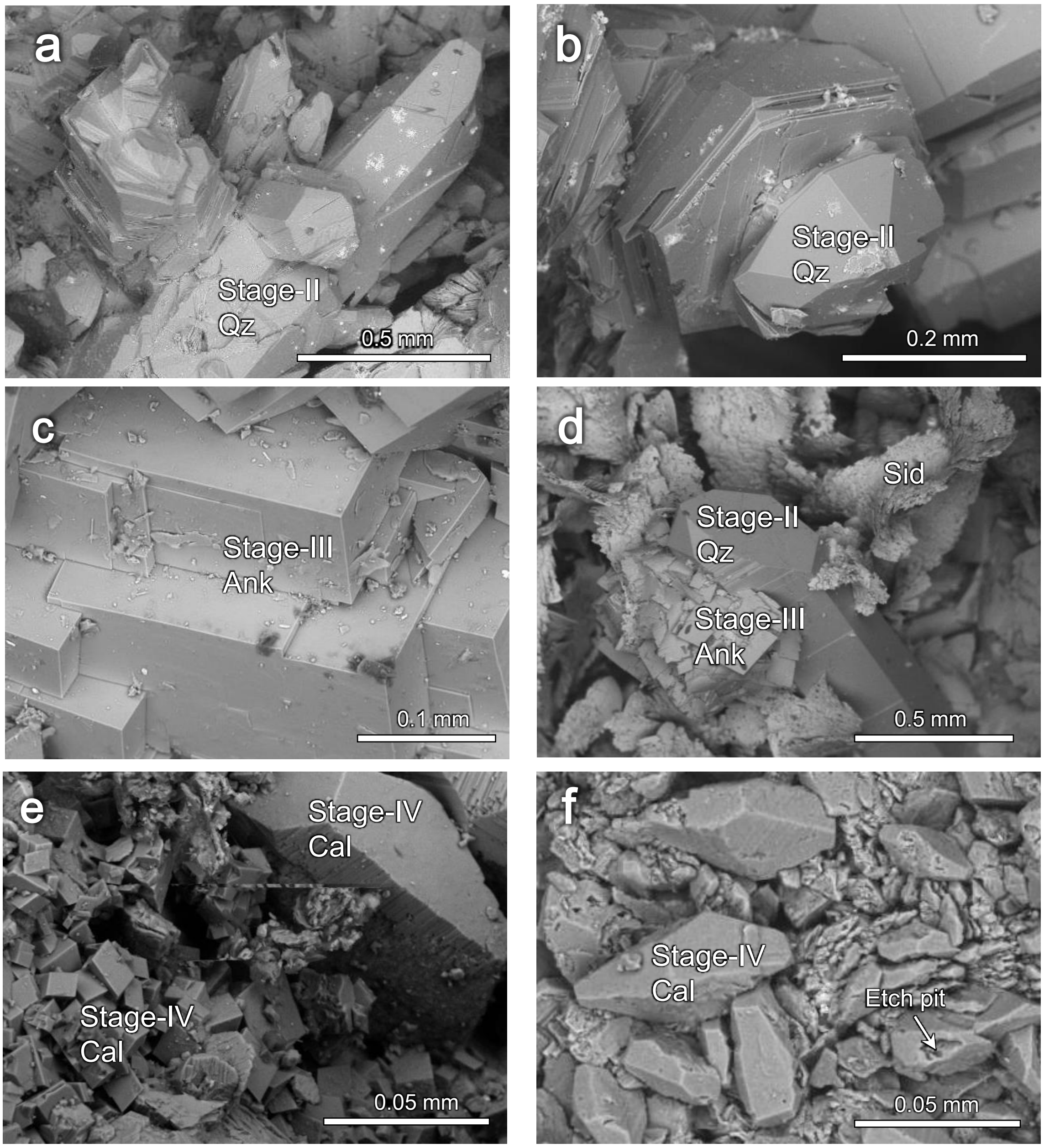
a
Stage-II
Qz
0.5 mm
b
Stage-II
Qz
0.2 mm
c
Stage-III
Ank
0.1 mm
d
Sid
Stage-II
Qz
Stage-III
Ank
0.5 mm
e
Stage-IV
Cal
Stage-IV
Cal
0.05 mm
f
Stage-IV
Cal
Etch pit
0.05 mm

Figure 8

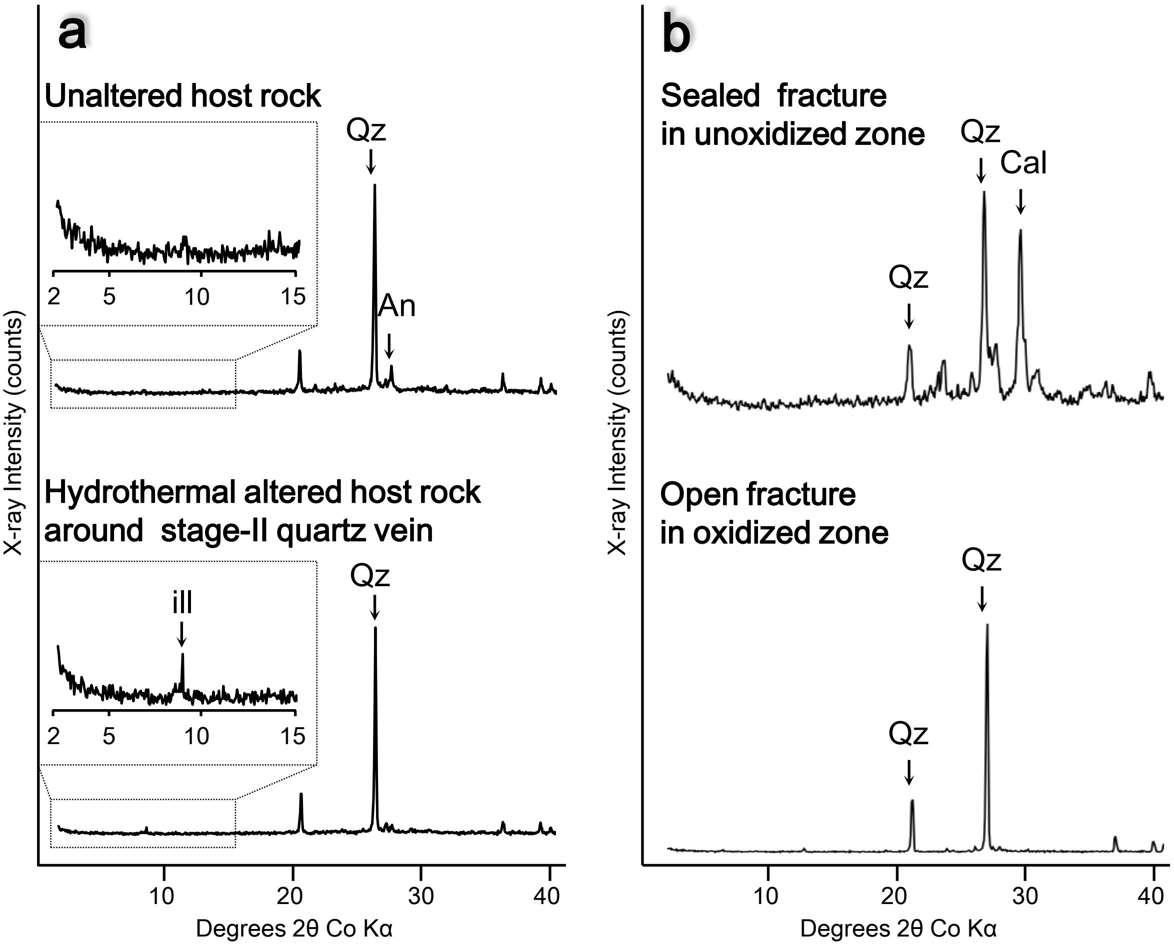
a
Unaltered host rock
Qz
An
2
5
10
15
Hydrothermal altered host rock
around stage-II quartz vein
Qz
ill
2
5
10
15
X-ray Intensity (counts)
10
20
30
40
Degrees 2θ Co Kα
b
Sealed fracture
in unoxidized zone
Qz
Cal
Qz
Open fracture
in oxidized zone
Qz
Qz
X-ray Intensity (counts)
10
20
30
40
Degrees 2θ Co Kα

Figure 9

Figure 10

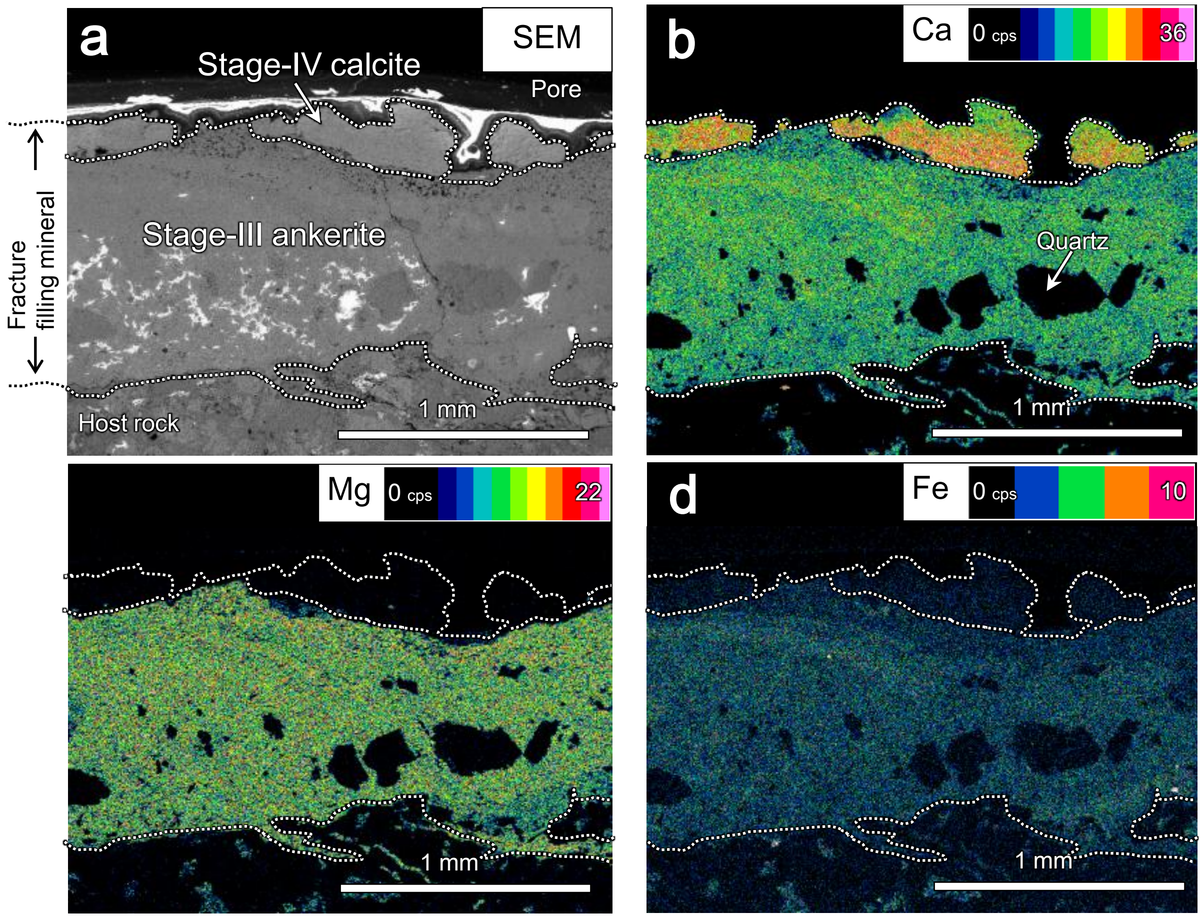

Figure 10

Figure 11

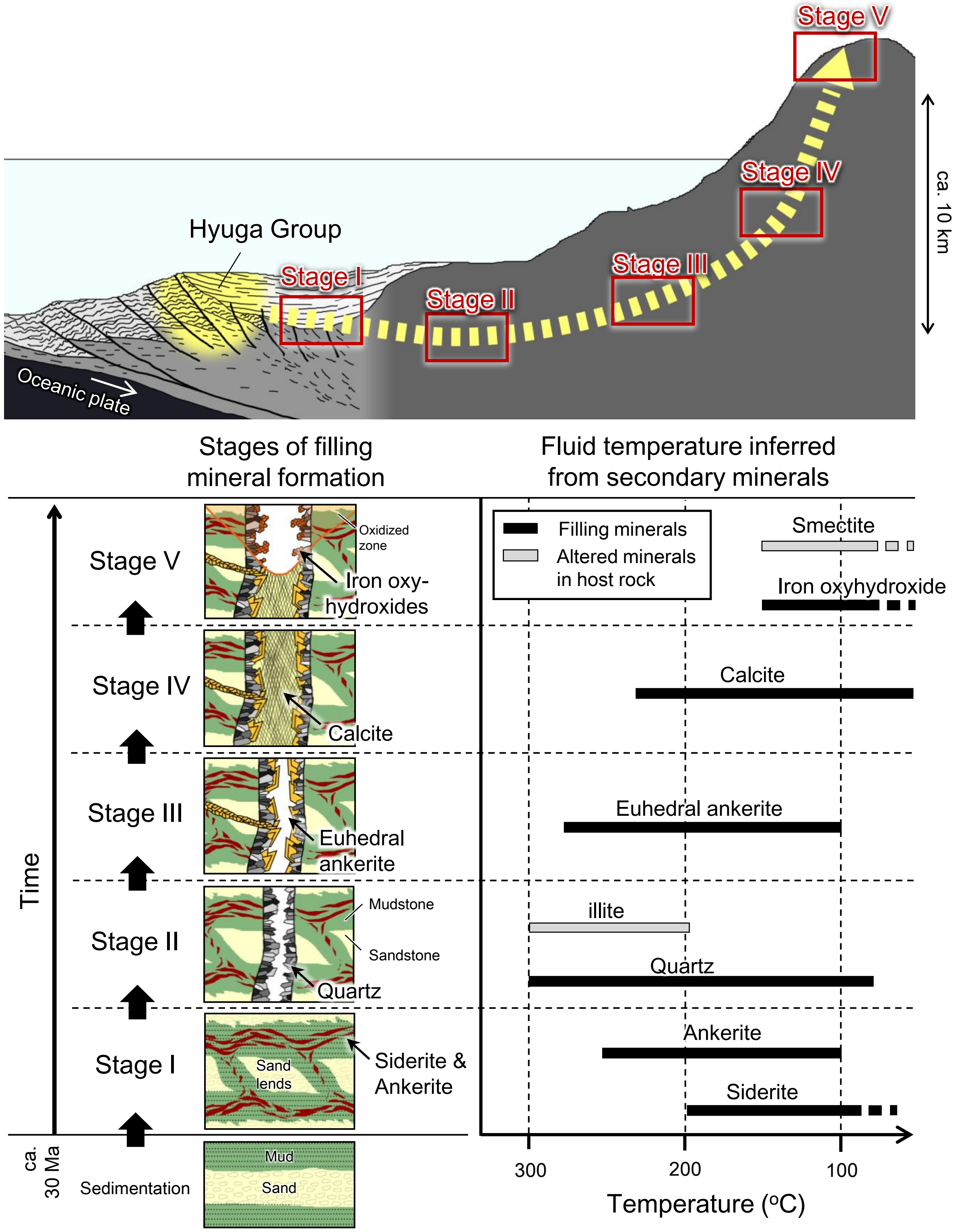

Figure 11

Table 1

Table 1

Depth	Core-A			Core-B			Core-C			Core-D			Core-E		
(m)	Of	Sf	Ox	Of	Sf	Ox	Of	Sf	Ox	Of	Sf	Ox	Of	Sf	Ox
0 - 1	18	0	1.0	9	0	1.0	–	–	–	7	0	0.8	5	0	1.0
1 - 2	13	0	1.0	13	0	0.9	–	–	–	11	0	0.6	7	0	1.0
2 - 3	5	0	0.5	9	0	1.0	–	–	–	16	0	0.8	13	0	0.4
3 - 4	9	0	0.8	8	0	1.0	–	–	–	11	0	0.5	11	0	0.8
4 - 5	8	0	0.7	11	0	0.9	–	–	–	9	2	0.5	8	0	1.0
5 - 6	10	0	1.0	15	0	0.6	–	–	–	5	0	0.2	5	0	0.5
6 - 7	9	0	0.9	14	0	0.9	–	–	–	9	0	0.9	9	0	0.7
7 - 8	8	0	1.0	13	0	1.0	–	–	–	4	0	0.0	4	0	0.7
8 - 9	9	0	0.7	14	0	0.9	–	–	–	1	1	0.0	0	0	0.0
9 - 10	13	0	1.0	2	0	0.6	–	–	–	5	0	0.1	7	0	0.7
10 - 11	14	0	1.0	7	0	0.7	–	–	–	1	1	0.1	7	0	0.5
11 - 12	11	0	1.0	8	0	1.0	–	–	–	12	0	0.5	5	0	0.4
12 - 13	6	0	0.5	15	0	0.8	–	–	–	6	6	0.3	2	0	0.4
13 - 14	5	0	0.3	7	0	0.7	–	–	–	7	7	0.4	7	0	0.8
14 - 15	9	0	1.0	2	0	0.2	–	–	–	10	2	0.2	6	0	0.6
15 - 16	6	0	0.8	12	0	0.7	–	–	–	6	3	0.0	–	–	–
16 - 17	3	0	0.2	8	0	0.9	–	–	–	5	2	0.1	–	–	–
17 - 18	0	2	0.0	9	0	0.7	–	–	–	10	5	0.3	–	–	–
18 - 19	5	1	0.4	8	0	0.6	–	–	–	11	2	0.1	–	–	–
19 - 20	5	0	0.8	12	0	0.7	–	–	–	10	0	0.2	–	–	–
20 - 21	7	0	0.7	10	0	0.7	–	–	–	0	11	0.0	8	0	0.8
21 - 22	11	0	0.9	7	0	0.8	–	–	–	2	3	0.0	16	0	0.9
22 - 23	10	0	0.7	10	0	0.9	–	–	–	2	10	0.0	13	0	0.8
23 - 24	7	0	0.6	13	0	1.0	–	–	–	0	6	0.1	11	0	0.5
24 - 25	3	0	0.3	15	0	1.0	–	–	–	6	6	0.1	10	0	0.5
25 - 26	4	1	0.5	13	0	1.0	4	3	0.3	7	4	0.2	13	0	0.6
26 - 27	11	0	0.3	13	0	0.6	0	5	0.0	1	1	0.1	8	0	0.9
27 - 28	9	0	0.5	10	0	0.6	0	6	0.0	9	9	0.0	18	0	0.9
28 - 29	14	3	0.4	9	0	0.8	0	4	0.0	0	6	0.1	8	0	1.0
29 - 30	15	0	0.8	16	0	1.0	0	3	0.0	3	14	0.0	12	0	0.9
30 - 31	6	1	0.5	14	0	0.8	0	12	0.0	–	–	–	3	0	0.6
31 - 32	9	0	0.7	9	0	0.5	0	14	0.0	–	–	–	5	0	0.5
32 - 33	10	2	0.5	3	0	0.3	0	8	0.1	–	–	–	8	0	0.8
33 - 34	16	0	0.6	12	0	0.8	0	14	0.1	–	–	–	8	0	0.9
34 - 35	7	2	0.3	4	1	0.2	5	5	0.0	–	–	–	2	0	0.2
35 - 36	8	0	0.2	13	0	0.3	0	9	0.0	–	–	–	0	0	0.0
36 - 37	8	2	0.4	9	0	0.2	0	6	0.0	–	–	–	8	0	0.7
37 - 38	2	6	0.3	10	0	0.4	0	9	0.0	–	–	–	9	0	0.8
38 - 39	5	5	0.3	8	0	0.2	0	6	0.0	–	–	–	9	0	0.6
39 - 40	4	7	0.2	3	8	0.1	0	9	0.0	–	–	–	5	0	0.3
40 - 41	3	1	0.3	0	11	0.0	2	6	0.1	–	–	–	5	0	0.5
41 - 42	1	0	0.1	3	7	0.0	0	6	0.0	–	–	–	4	0	0.4
42 - 43	7	0	0.1	1	1	0.0	0	14	0.0	–	–	–	8	0	0.6
43 - 44	5	5	0.2	2	2	0.0	2	6	0.0	–	–	–	11	0	0.6
44 - 45	2	4	0.1	2	2	0.2	3	6	0.1	–	–	–	15	0	0.8
45 - 46	0	7	0.0	8	0	0.2	4	6	0.1	–	–	–	14	0	0.7
46 - 47	0	0	0.0	0	7	0.1	3	5	0.0	–	–	–	11	0	0.4
47 - 48	0	0	0.0	2	2	0.1	0	4	0.0	–	–	–	10	0	0.3
48 - 49	4	4	0.0	0	16	0.1	0	2	0.0	–	–	–	13	0	0.0
49 - 50	2	2	0.1	0	8	0.0	0	1	0.0	–	–	–	12	0	0.1
50 - 51	5	0	0.1	0	8	0.0	–	–	–	–	–	–	12	0	0.1
51 - 52	2	2	0.0	3	9	0.0	–	–	–	–	–	–	8	0	0.1
52 - 53	6	0	0.0	5	5	0.3	–	–	–	–	–	–	4	0	0.0
53 - 54	4	4	0.0	1	11	0.0	–	–	–	–	–	–	12	0	0.2
54 - 55	7	0	0.1	9	9	0.2	–	–	–	–	–	–	8	0	0.5
55 - 56	5	5	0.2	8	2	0.0	–	–	–	–	–	–	2	2	0.0
56 - 57	1	1	0.1	4	0	0.0	–	–	–	–	–	–	10	2	0.0
57 - 58	0	0	0.0	6	6	0.2	–	–	–	–	–	–	7	0	0.3
58 - 59	0	2	0.0	5	9	0.2	–	–	–	–	–	–	11	0	0.1
59 - 60	0	0	0.0	5	5	0.1	–	–	–	–	–	–	8	0	0.3
60 - 61	–	–	–	4	7	0.0	–	–	–	–	–	–	4	3	0.2
61 - 62	–	–	–	0	9	0.0	–	–	–	–	–	–	8	0	0.3
62 - 63	–	–	–	0	10	0.0	–	–	–	–	–	–	7	0	0.2
63 - 64	–	–	–	0	15	0.0	–	–	–	–	–	–	0	3	0.1
64 - 65	–	–	–	0	9	0.0	–	–	–	–	–	–	0	4	0.0
65 - 66	0	9	0.0	6	6	0.1	–	–	–	–	–	–	0	0	0.0
66 - 67	6	6	0.1	0	2	0.0	–	–	–	–	–	–	7	0	0.2
67 - 68	2	2	0.0	3	8	0.1	–	–	–	–	–	–	3	0	0.0
68 - 69	0	1	0.0	2	5	0.0	–	–	–	–	–	–	0	3	0.0
69 - 70	0	12	0.0	10	0	0.1	–	–	–	–	–	–	2	2	0.1
70 - 71	5	0	0.0	5	5	0.0	–	–	–	–	–	–	1	6	0.1
71 - 72	4	4	0.1	4	9	$\boxed{0.1}$ Core-B 72 m	–	–	–	–	–	–	0	2	0.0
72 - 73	0	2	0.0	0	9	0.0	–	–	–	–	–	–	7	0	0.0
73 - 74	4	0	0.1	0	8	0.0	–	–	–	–	–	–	0	10	0.0
74 - 75	0	0	0.0	0	6	0.0	–	–	–	–	–	–	2	8	0.0
75 - 76	0	2	0.0	–	–	–	–	–	–	–	–	–	0	7	$\boxed{0.1}$ Core-E 76 m
76 - 77	3	3	0.0	–	–	–	–	–	–	–	–	–	0	5	0.0
77 - 78	4	5	$\boxed{0.2}$ Core-A 78 m	–	–	–	–	–	–	–	–	–	1	2	0.0
78 - 79	0	2	0.0	–	–	–	–	–	–	–	–	–	0	6	0.0
79 - 80	3	3	0.0	–	–	–	–	–	–	–	–	–	0	3	0.0
80 - 81	0	1	0.0	5	5	0.0	–	–	–	–	–	–	0	7	0.0
81 - 82	0	1	0.0	0	13	0.0	–	–	–	–	–	–	1	2	0.0
82 - 83	3	0	0.0	0	1	0.0	–	–	–	–	–	–	0	5	0.0
83 - 84	0	4	0.0	0	12	0.0	–	–	–	–	–	–	0	6	0.0
84 - 85	0	9	0.0	0	13	0.0	–	–	–	–	–	–	0	5	0.0
85 - 86	0	7	0.0	0	5	0.0	–	–	–	–	–	–	0	3	0.0
86 - 87	0	4	0.0	0	4	0.0	–	–	–	–	–	–	0	9	0.0
87 - 88	0	3	0.0	0	7	0.0	–	–	–	–	–	–	0	5	0.0
88 - 89	0	5	0.0	0	6	0.0	–	–	–	–	–	–	0	7	0.0
89 - 90	0	5	0.0	2	5	0.0	–	–	–	–	–	–	5	14	0.0
90 - 91	0	7	0.0	3	12	0.0	–	–	–	–	–	–	4	4	0.0
91 - 92	0	3	0.0	0	8	0.0	–	–	–	–	–	–	0	5	0.0
92 - 93	3	5	0.0	1	3	0.0	–	–	–	–	–	–	0	3	0.0
93 - 94	0	6	0.0	0	4	0.0	–	–	–	–	–	–	3	3	0.0
94 - 95	0	2	0.0	2	16	0.0	–	–	–	–	–	–	3	14	0.0
95 - 96	0	6	0.0	1	7	0.0	–	–	–	–	–	–	0	2	0.0
96 - 97	0	1	0.0	1	4	0.0	–	–	–	–	–	–	0	0	0.0
97 - 98	3	3	0.0	0	10	0.0	–	–	–	–	–	–	0	7	0.0
98 - 99	2	2	0.0	1	4	0.0	–	–	–	–	–	–	0	4	0.0
99 - 100	0	9	0.0	0	7	0.0	–	–	–	–	–	–	1	2	0.0
100 - 101	0	3	0.0	–	–	–	–	–	–	–	–	–	2	8	0.0
101 - 102	0	6	0.0	–	–	–	–	–	–	–	–	–	0	6	0.0
102 - 103	0	16	0.0	–	–	–	–	–	–	–	–	–	1	7	0.0
103 - 104	3	5	0.0	–	–	–	–	–	–	–	–	–	3	8	0.0
104 - 105	3	1	0.0	–	–	–	–	–	–	–	–	–	0	10	0.0
105 - 106	0	16	0.0	–	–	–	–	–	–	–	–	–	2	12	0.0
106 - 107	0	8	0.0	–	–	–	–	–	–	–	–	–	0	4	0.0
107 - 108	0	8	0.0	–	–	–	–	–	–	–	–	–	0	7	0.0
108 - 109	0	1	0.0	–	–	–	–	–	–	–	–	–	0	12	0.0
109 - 110	0	3	0.0	–	–	–	–	–	–	–	–	–	0	10	0.0
110 - 111	3	0	0.0	–	–	–	–	–	–	–	–	–	0	18	0.0
111 - 112	0	4	0.0	–	–	–	–	–	–	–	–	–	0	15	0.0
112 - 113	0	2	0.0	–	–	–	–	–	–	–	–	–	0	3	0.0
113 - 114	0	2	0.0	–	–	–	–	–	–	–	–	–	0	9	0.0
114 - 115	0	1	0.0	–	–	–	–	–	–	–	–	–	2	6	0.0
115 - 116	0	3	0.0	–	–	–	–	–	–	–	–	–	2	3	0.0
116 - 117	1	3	0.0	–	–	–	–	–	–	–	–	–	2	11	0.0
117 - 118	3	7	0.0	–	–	–	–	–	–	–	–	–	0	10	0.0
118 - 119	2	2	0.0	–	–	–	–	–	–	–	–	–	2	1	0.0
119 - 120	0	7	0.0	–	–	–	–	–	–	–	–	–	0	7	0.0
120 - 121	0	9	0.0	–	–	–	–	–	–	–	–	–	–	–	–
121 - 122	3	5	0.0	–	–	–	–	–	–	–	–	–	–	–	–
122 - 123	0	5	0.0	–	–	–	–	–	–	–	–	–	–	–	–
123 - 124	3	5	0.0	–	–	–	–	–	–	–	–	–	–	–	–
124 - 125	0	7	0.0	–	–	–	–	–	–	–	–	–	–	–	–
125 - 126	2	5	0.0	–	–	–	–	–	–	–	–	–	–	–	–
126 - 127	2	7	0.0	–	–	–	–	–	–	–	–	–	–	–	–
127 - 128	0	4	0.0	–	–	–	–	–	–	–	–	–	–	–	–
128 - 129	0	0	0.0	–	–	–	–	–	–	–	–	–	–	–	–
129 - 130	0	2	0.0	–	–	–	–	–	–	–	–	–	–	–	–
130 - 131	0	3	0.0	–	–	–	–	–	–	–	–	–	–	–	–
131 - 132	0	1	0.0	–	–	–	–	–	–	–	–	–	–	–	–
132 - 133	0	3	0.0	–	–	–	–	–	–	–	–	–	–	–	–
133 - 134	0	4	0.0	–	–	–	–	–	–	–	–	–	–	–	–
134 - 135	1	6	0.0	–	–	–	–	–	–	–	–	–	–	–	–
135 - 136	1	6	0.0	–	–	–	–	–	–	–	–	–	–	–	–
136 - 137	0	6	0.0	–	–	–	–	–	–	–	–	–	–	–	–
137 - 138	0	0	0.0	–	–	–	–	–	–	–	–	–	–	–	–
138 - 139	0	1	0.0	–	–	–	–	–	–	–	–	–	–	–	–
139 - 140	1	7	0.0	–	–	–	–	–	–	–	–	–	–	–	–

Of: Open fracture frequency Sf: Sealed fracture frequency Ox: Oxidized zone distribution ratio $\boxed{0.1}$: Deepest oxidized zone

Table 2

Depth (m)	Litho logy	Major Elements XRF (wt%)										IL (wt%)	Total (wt%)
		SiO_2	TiO_2	Al_2O_3	Fe_2O_3*	MnO	MgO	CaO	Na_2O	K_2O	P_2O_5		
0.9	Ss	76.20	0.44	11.12	2.91	0.013	0.90	0.12	2.58	2.54	0.088	1.61	98.51
8.5	Ss	79.41	0.43	10.11	1.90	0.003	0.66	0.13	2.22	2.44	0.048	1.69	99.05
13.2	Ss	78.10	0.49	10.10	2.33	0.009	0.75	0.18	2.26	2.31	0.054	2.23	98.81
22.3	Ss	78.78	0.55	10.67	2.74	0.035	0.93	0.28	2.47	2.43	0.103	1.51	100.48
28.9	Ss	77.79	0.47	10.47	1.97	0.007	0.74	0.18	2.34	2.44	0.082	2.48	98.97
31.8	Ss	74.37	0.53	9.96	2.97	0.052	1.05	2.53	2.38	2.12	0.114	3.01	99.08
38.5	Ms	62.30	0.81	17.43	5.72	0.043	2.50	0.27	1.16	4.70	0.128	4.45	99.51
43.7	Ss	71.63	0.53	12.47	3.57	0.029	1.30	0.98	2.56	2.88	0.113	2.35	98.40
48.4	Ms	61.92	0.79	16.03	5.91	0.047	2.36	1.76	1.34	4.13	0.149	4.72	99.15
51.4	Ss	71.55	0.31	8.03	2.93	0.090	0.81	4.00	2.09	1.75	0.079	4.04	95.68
59.6	Ss	70.98	0.49	9.33	3.48	0.038	1.25	2.79	2.19	1.90	0.116	3.50	96.06
62.8	Ss	79.40	0.45	9.46	2.41	0.027	0.79	0.36	2.29	2.37	0.088	1.42	99.07
67.3	Ss	75.55	0.41	10.27	2.86	0.024	1.02	1.48	2.42	2.51	0.087	2.48	99.10
72.8	Ss	76.30	0.45	9.42	2.25	0.025	0.75	1.32	2.21	2.54	0.085	2.14	97.49
77.5	Ss	76.48	0.37	9.56	2.41	0.042	0.84	2.11	2.38	2.45	0.103	2.65	99.38
84.5	Ss	73.44	0.46	10.47	2.86	0.032	0.92	1.71	2.31	2.71	0.097	2.51	97.51
88.5	Ss	75.44	0.41	9.10	2.55	0.035	0.78	1.90	2.06	2.41	0.083	2.43	97.18
94.9	Ss	75.93	0.37	9.70	2.74	0.038	0.95	1.95	2.33	2.40	0.086	2.60	99.08
102.9	Ss	74.02	0.42	11.24	2.41	0.026	0.66	0.63	2.14	3.08	0.093	2.98	97.69
110.2	Ss	77.84	0.32	9.34	2.34	0.032	0.82	1.05	2.48	2.12	0.087	2.96	99.38
115.8	Ss	79.18	0.41	9.23	1.92	0.018	0.54	0.71	2.42	2.34	0.092	2.41	99.25

Ss: Sandstone Ms: Mudstone *) Total iron as Fe_2O_3